Vacuum 207 (2023) 111658

Contents lists available at ScienceDirect

Vacuum

journal homepage: www.elsevier.com/locate/vacuum

X-ray ultrashort pulse emission characteristic of carbon nanotube cold cathode X-ray source by pulse driving mode

Sheng Lai [a], Yunpeng Liu [a,b,**], Junxu Mu [a], Zhaopeng Feng [a], Kai Miao [a], Xiaobin Tang [a,b,*]

[a] Department of Nuclear Science and Technology, Nanjing University of Aeronautics and Astronautics, Nanjing, 210016, China
[b] Key Laboratory of Nuclear Technology Application and Radiation Protection in Astronautics, Ministry of Industry and Information Technology, Nanjing, 210016, China

ARTICLE INFO

Keywords:
Carbon nanotube
X-ray source
Pulse emission characteristic
Pulse driving mode

ABSTRACT

In the present work, we build a triode structure of carbon nanotube (CNT) cold cathode X-ray source driven by pulse voltage in dynamic vacuum system. The results show that the grid voltage and pulse width affect the amplitude, delay time and relative pulse spread of X-ray. The X-ray emission delay time decreases sharply from 102 to 75 ns when the grid voltage increases from 600 to 650 V. The relative pulse spread tends to be saturated with approximately 350 ns (±20 ns) when the voltage increases from 600 to 650 V. The theoretical limit frequency of this X-ray pulsed emission system is approximately 2.86 MHz (1/350 ns). This work reveals the ultrashort pulse emission characteristics and affecting factors of CNT cold cathode X-ray source, promoting the development of CNT cold cathode X-ray source in pulse application.

Pulse X-ray source is important for pulse application, such as X-ray communication (XCOM), high-speed imaging and basic physics/chemistry science because of its the unique pulse working mode [1–4]. Small and compact X-ray sources, such as hot cathode, photocathode, and cold cathode X-ray sources, can be used in XCOM or high-speed imaging [5–7]. However, compared with hot cathode and photocathode, CNT cold cathode X-ray source has the advantages of large current, controllable emission, and low power consumption [8,9]. Therefore, the CNT cold cathode X-ray source has great potential for this application. Some researchers have studied cold cathode pulse emission. Kang et al. [10] adopted active-current control method to realize cold cathode pulse emission. The results showed that resistance could remarkably decrease the pulse emission response time. Yue et al. [11] carried out pulse diagnostic imaging experiment and found an obvious time delay between X-ray and pulse voltage. Lei et al. [12] obtained that the imaging quality was positively correlated with the X-ray intensity based on metronome pulse imaging experiment. Han et al. [13] studied the high current emission mode of CNT film at 1 kHz with 10% duty cycle, and the results showed that CNT films had a good lifetime under pulse emission condition, but the pulsed X-ray emission characteristics were still unclear. Golden Engineering, Inc [14]. developed an ultrashort pulse cold cathode X-ray source of a minimum pulse width of 10 ns, but the pulse frequency was just several Hz. The delay time of X-ray waveform has been observed, and the amplitude of X-ray waveform was attenuated based on high-frequency XCOM experiment [15]. These researchers have not dig into the detail of the emission characteristics and affecting factors of pulsed X-ray source. The emission characteristics of pulsed X-ray, such as amplitude, delay time and pulse spread, affect X-ray applications, including signal synchronization of multiple emission arrays [15], instantaneous image capture of high-speed imaging [16], and transient analysis of chemical reaction and plasma [17]. Therefore, the emission characteristics and affecting factors of CNT cold cathode pulse X-ray source are not clear, especially in ultrashort pulse X-ray emission in this work.

In this work, a triode structure is built in a dynamic vacuum system to study the emission characteristics and affecting factors of X-ray by pulse driving mode. This work reveals the emission characteristics and affecting factors of field emission ultrashort pulse X-ray system, and promotes the development of CNT cold cathode pulse X-ray source technology.

The triode structure and circuit of CNT cold cathode are built in a dynamic vacuum system, as shown in Fig. 1(a). The CNT cold cathode electron source and the anode target are placed inside and connected to those external equipments through the electrode flange. During the experiment, the vacuum level of the system is maintained in the order of 10^{-6} Pa. Fig. 1(b) is the pulse emission process diagram of CNT cold

* Corresponding author. Department of Nuclear Science and Technology, Nanjing University of Aeronautics and Astronautics, Nanjing, 210016, China.
** Corresponding author. Department of Nuclear Science and Technology, Nanjing University of Aeronautics and Astronautics, Nanjing, 210016, China.
E-mail addresses: liuyp@nuaa.edu.cn (Y. Liu), tangxiaobin@nuaa.edu.cn (X. Tang).

https://doi.org/10.1016/j.vacuum.2022.111658
Received 29 August 2022; Received in revised form 11 October 2022; Accepted 3 November 2022
Available online 10 November 2022

cathode. The grid and cathode is connected to the pulse power supply and ground, respectively. The anode is a copper target and connectes to high-voltage power supply, and the inclination angle of the target is 15°. The diameter of CNT cold cathode is approximately 5 mm, and the cathode–grid distance is 200 μm. Pulse emission electron of CNT cold cathode is controlled by pulse power supply. CNT cold cathode emits electrons when the pulse power supply is on high level, and no electrons in low level. The single pulse of pulse power supply is set, with the pulse width of several hundred nanosecond, as well as the pulse amplitude of several hundred voltage in the experiment.

The CNT cold cathode is prepared via screen printing method by using molybdenum as cathode substrate. Scanning electron microscopy (SEM) and transmission electron microscopy (TEM) are used to characterize the CNT cold cathode, as shown in Fig. 2. The surface morphology characteristics indicate that CNT is distributed unevenly on the cathode surface, as shown in Fig. 2(a). Most CNTs creep on the substrate surface, and only a small part extends out of the surface, which is the key part for electron emission. The diameter of multi-walled CNT is approximately 10–20 nm, and approximately 10 wall layers are observed, as shown in Fig. 2(b).

The X-ray detector used in this study is a self-made lutetium–yttrium oxyorthosilicate (LYSO) scintillator coupled with silicon photomultiplier (SiPM) high-frequency-sensitive photodetector [18]. The detector used in the experiment is array LYSO-SiPM X-ray detector. The length and width of each LYSO crystal are about 3 mm for matching the photosensitive area of SiPM, and the thickness is approximately 5 mm. The transmission coefficient of X-ray photo from LYSO to SiPM is above 0.8, that means more than 80% of the scintillation photons reaching the exit surface could enter SiPM. The I–V curve and Fowler–Nordheim (F–N) formula verification of CNT cold cathode are discussed first, as shown in Fig. 3.

The current is measured by external resistance of pulse grid voltage. Considering that the pulse emission current from CNT cathode is relatively small, a high resistance is necessary to measure the loss of voltage. The high-frequency non-inductive resistance value is 100 kΩ, and the pulse frequency of pulse power supply is 10 kHz with 40% duty cycle. The current increases exponentially, which is consistent with the field emission characteristics, as shown in Fig. 3(a). According to the F–N formula:

$$J = \frac{AE^2}{\varnothing}\exp\left(-\frac{B\varnothing^{\frac{3}{2}}}{E}\right) \tag{1}$$

After transformation,

$$\ln\left(\frac{J}{E^2}\right) = -B\varnothing^{\frac{3}{2}}\frac{1}{E} + \ln\left(\frac{A}{\varnothing}\right), \tag{2}$$

where J is the current density, E is the cathode electric field strength, $\varnothing$ is the work function of CNT, and A and B are constants. From formula (2), the variability law between the ln(J/E2) and the 1/E shows a linear relationship. Two slopes are observed in the high- and low-current emission, as shown in Fig. 3(b) (blue and green part, respectively). The electric field intensity of blue part, where the current is large, is higher than that of green part. After analyzing deeply about the double slopes of the curve shape, it can be considered that one of an important reasons is the large resistance. In the high current emission mode, it has a large relative voltage drop on the resistor and leads to a weakening of electric field strength on CNT cathode. In addition, the local electric field strength is also weakened due to the space charge shielding effect [19], which restricts the electron emission.

In order to reduce the influence factors of X-ray pulse emission process, we abandon the large resistance of the cathode circuit, so the cathode is directly grounded in the next experiment. First, the relationship of X-ray waveform amplitude versus pulse width is discussed, as shown in Fig. 4. The experimental results show that the amplitude of X-ray waveform increases rapidly with the increase of pulse width, and the X-ray waveform reaches the peak at 300 ns pulse width at the grid voltage of 600 V.

To characterize the square wave saturation of X-ray waveform, we adopt the ratio of peak width. The ratio of peak width is the ratio of the peak horizontal part of X-ray waveform to the peak horizontal part of pulse power supply waveform. The ratio increases with the increase of pulse width, as shown in Fig. 4 green line. The wider the voltage pulse width, the fuller the X-ray waveform, and the X-ray shape gradually becomes square. When the pulse width is lower than 1000 ns, the peak width of X-ray waveform is shorter than that of voltage waveform, so the ratio of peak width is below 1, as shown in Fig. 4 green line. This result indicates that the CNT cathode emits fewer electrons under the condition of short pulse width, which leads to waveform distortion and does not reach saturation.

To study the X-ray ultrashort pulse emission characteristic, we discuss the waveform amplitude, delay time and relative pulse spread of pulse X-ray, the results as shown in Fig. 5.

The result indicates that the amplitude of X-ray waveform increases with the increase of grid voltage, as shown in Fig. 5(a) solid line. The pulse width has obvious influence on the X-ray waveform amplitude, which is always higher at 200 ns pulse width than that at 100 ns. The X-ray waveform amplitude peaks at 2.7 V under the condition of 630 V at 200 ns, while it only reaches half the amplitude under 100 ns pulse width. The X-ray waveform amplitude reaches the peak when the grid voltage reaches 650 V under 100 ns pulse width. The X-ray waveform is fuller at 200 ns pulse width than that at 100 ns pulse width, as shown in the experimental diagram of Fig. 5 (a1) and (a2). This finding is

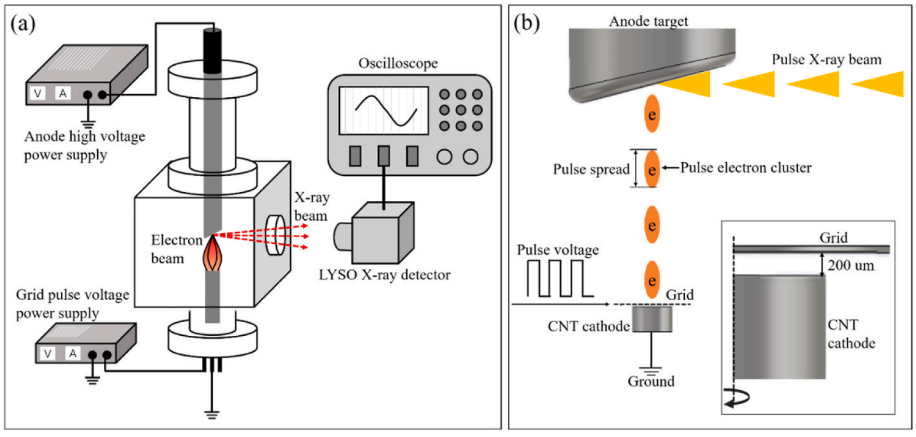

Fig. 1. CNT cold cathode X-ray source in dynamic vacuum system, a): measure circuit structure; b): electron pulse emission process. The insert diagram in (b) is the local drawing of CNT cold cathode.

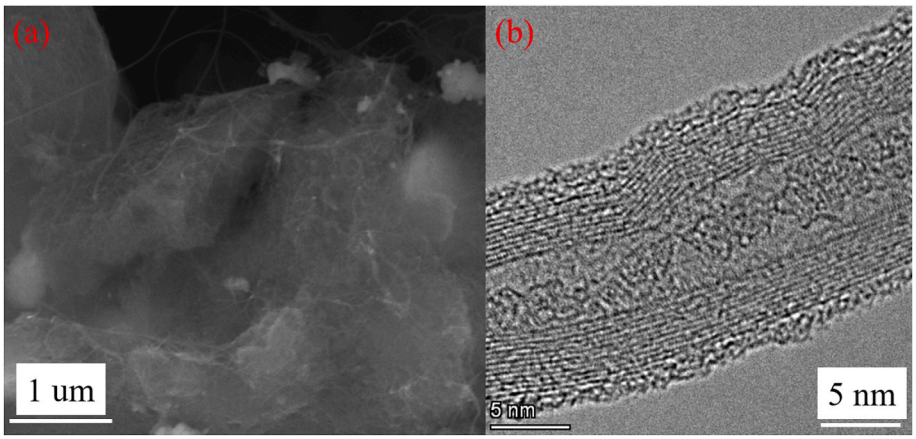

Fig. 2. Characterization of CNT cold cathode, a): SEM scale in 1 μm; b): TEM scale in 5 nm.

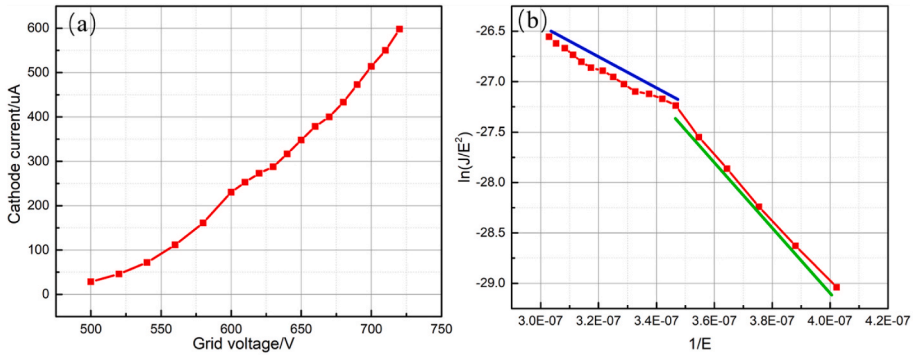

Fig. 3. Electron emission characteristics of CNT cold cathode, a): I–V curve; b) F–N theoretical verification.

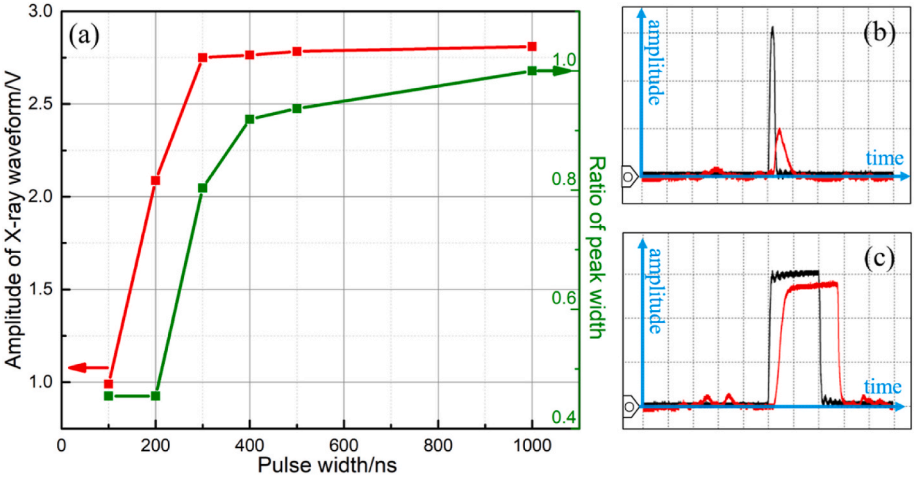

Fig. 4. a) Relationship of X-ray waveform amplitude and pulse width. Experimental results under different conditions of b) 600 V at 100 ns and c) 600 V at 1000 ns. The black line refers to the voltage waveform of the grid, in which the red line denotes the X-ray waveform. Longitudinal scales of black and red lines are 200 and 1 V in (b) and (c), respectively. Each grid of horizontal axis time scale is 500 ns in (b) and (c). The anode voltage is maintained at 25 kV.

obtained, because the pulse width greatly affects the number of electron beams emitted from the cathode, resulting in more X-ray photons. Therefore, the X-ray waveform amplitude is higher, and the waveform shape is more saturated than that in short pulse width.

The delay time is determined that the time from the rise of pulse power supply waveform to the rise of X-ray waveform. With the increase of pulse voltage, the delay time of X-ray waveform decreases under the pulse voltage range of 600–650 V, as shown in Fig. 5(a) dotted line. The delay time of Fig. 5 (a) is the average value through calculating multiple groups of data. The delay time of X-ray waveform decreases from 100 to 75 ns when the grid voltage increases from 600 to 650 V under the experimental conditions of pulse widths of 100 and 200 ns. Through analysis, the components of X-ray emission delay time included 1) the time of pulse power supply rising edge (T1), 2) the time of electron escaping the material (T2), 3) the time of charging effect of cathode-grid capacitor (T3), 4) the transit-time of electron from cathode to anode

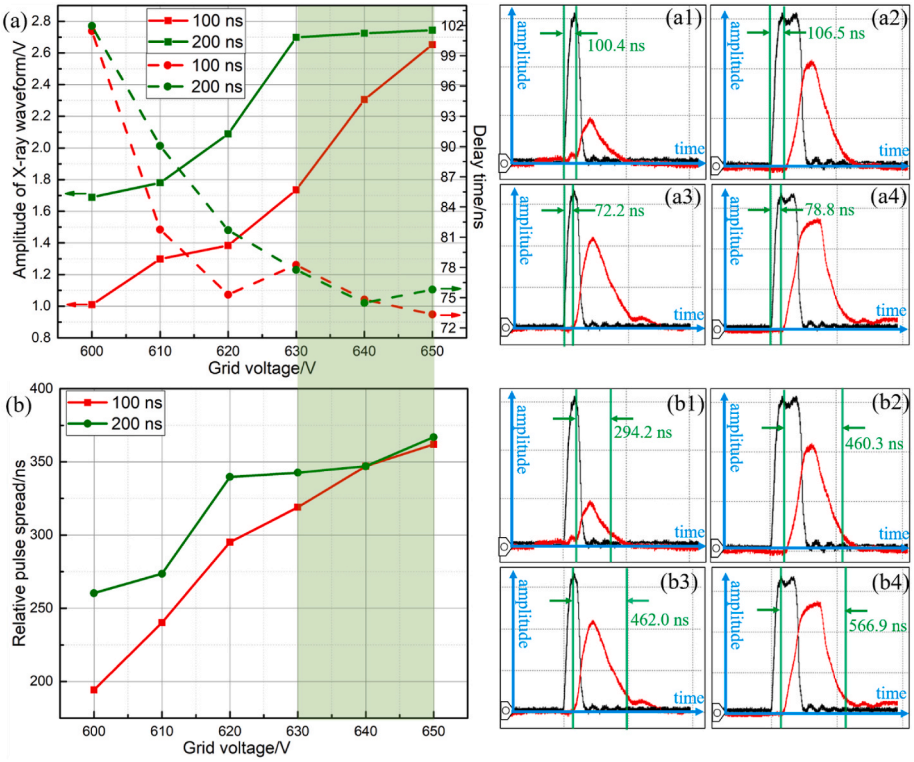

Fig. 5. X-ray ultrashort pulse emission amplitude and time characteristics of CNT cold cathode X-ray source. a) Relationship of X-ray waveform amplitude and delay time versus grid voltage. b) Relationship of X-ray waveform relative pulse spread versus grid voltage. Experimental results under different gird voltage and pulse width: a1/b1) 600 V at 100 ns; a2/b2) 600 V at 200 ns; a3/b3) 650 V at 100 ns; and a4/b4) 650 V at 200 ns. The black line refers to the voltage waveform of the grid, the red line denotes the X-ray waveform. Longitudinal scales of black and red line are 200 and 1 V in (a1/b1), (a2/b2), (a3/b3), and (a4/b4), respectively. Each grid of horizontal axis time scale is 500 ns in (a1/b1), (a2/b2), (a3/b3) and (a4/b4). The anode voltage is maintained at 25 kV. The green vertical lines is represented a measurement time section.

(T4), 5) the time of X-ray producing from anode target (T5), 6) the time of X-ray transmission to X-ray detector (T6), 7) the time of X-ray detector responsing (T7). The components and values of X-ray emission delay time are shown in Table 1. Due to the close distance between cathode and grid (200 μm), the cathode and grid structure can be regarded as a capacitor. The capacitor charging effect will cause delay time during pulse emission. The capacitance value of the cathode-grid is approximately 114 pF by measurement. The resistance of cathode circuit including CNT substrate, electrode flange and wire is approximately several Ohms. Therefore, the maximum delay time RC caused by the capacitor charging effect of cathode-grid does not exceed 1–2 ns. Therefore, RC capacitor charging effect is not the main factor causing delay time. We measure the rising-time of pulse power supply waveform, and find that the rising-time is approximately 70–80 ns and 50–60 ns under the conditions of 600 V and 650 V, respectively. As we know, the field emission electron needs to reach sufficient electric field strength to be emitted from the cathode. Therefore, the rising-time of the pulse power supply plays a key role in the delay time of electron emission. Consequently, the rising-time of grid voltage mainly affects the pulse X-ray delay time through analysis deeply. The higher the pulse voltage, the shorter the delay time of X-ray. According to Ref. [20], the time of electron escaping from the material to the vacuum is very short, about on the order of femtosecond, so it can be ignored in this work. The transit time of electron from cathode to anode is approximately 0.679 ns calculated by the theory of vacuum electromagnetic field electron transport, which is a little affect on X-ray delay time. According to Ref. [21], the time of X-ray generated from anode target by electron bombardment is in range of 10^{-5}-1 ns, so it is a little affect on X-ray delay time. The time of X-ray transmission from the anode target to the X-ray detector does not exceed 0.5 ns by calculated, so this has little impact on X-ray delay time. After detector absorbs X-ray, a lot of primary and secondary ionization and excitation are produced in LYSO material. It will produce a variety of physical processes, including the migration of electron hole pairs, the coupling relaxation of electron and electron, electron and phonon, the capture of electron hole pairs, the energy transfer between charge carriers and luminescent centers and so on [22]. These processes can cause time delay of X-ray. Meanwhile, the photoelectric conversion and electronics processing in SiPM can also cause time delay. According to similar Ref. [23], it can be estimated that the X-ray delay time caused by LYSO-SiPM detector used in this experiment is approximately 20 ns. In summary, compared with the above seven delay time factors, the rising-time of the pulse power supply is the main factor for the X-ray delay time. Although the selection of pulse power supply with better performance can shorten the delay time caused by rising-time, the X-ray emission delay time can not be completely eliminated because T2, T3, T4, T5, T6, T7 are objective factors that can not be eliminated.

Table 1
The components and values of X-ray emission delay time.

Symbol	Meaning	Value	Source
T1	the time of pulse power supply rising edge	50–80 ns	experiment
T2	the time of electron escaping the material	~10^{-6} ns	Ref. [20]
T3	the time of charging effect of cathode-grid capacitor	<1–2 ns	experiment & calculation
T4	the transit-time of electron from cathode to anode	~0.679 ns	CST simulation & calculation
T5	the time of X-ray producing from anode target	~10^{-5}–1 ns	Ref. [21]
T6	the time of X-ray transmission to X-ray detector	<0.5 ns	calculation
T7	the time of X-ray detector responsing	~20 ns	Ref. [23]

We further research the pulse spread characteristics of X-ray waveform. The grid voltage has an obvious effect on X-ray waveforms pulse width under the experiment process. Under the condition of 200 ns and 100 ns pulse widths of the power supply, the X-ray pulse widened as 200 ns is always wider than that in 100 ns. In order to make the X-ray pulse width under the two different pulse widths comparable, the relative pulse spread is adopted. The relative pulse spread means the X-ray pulse width minus the pulse width of pulse power supply, the result as shown

in Fig. 5(b). Because the X-ray detector has fluorescence decay effect, a part of X-ray waveform in falling edge is not generated by real X-ray photon [18]. Therefore, the X-ray pulse width is defined as from the start of the rising edge to the peak amplitude of the falling edge of 10%, as shown in Fig. 5 (b1-b4). According to the experimental results, the relative pulse spread increases gradually with the increase of grid voltage, and when the X-ray waveform reaches the peak, the relative pulse spread of the X-ray waveform also tends to be saturated, and the relative pulse spread at saturation is approximately 350 ns (±20 ns), as shown in Fig. 5(b) from 630 to 650 V green part. It is mainly contributed by the rising and falling edges of the X-ray waveform. The shape of X-ray waveform is affected by the performances of pulse power supply and X-ray detector, which indicates the X-ray pulse emission system has a 350 ns (±20 ns) relative pulse spread. High signal-to-noise ratio of X-ray waveform is more favorable to X-ray practical application. Therefore, according to the analysis above, it can be inferred that the theoretical limit frequency of this field emission cold cathode X-ray source pulse emission system is approximately 2.86 MHz (1/350 ns). Exceeding this frequency, the waveforms may overlap and cannot be distinguished, which will cause error.

In the present study, a triode structure of CNT cold cathode is built in the dynamic vacuum system, and the X-ray pulse emission characteristics and affecting factors of CNT cold cathode are studied by ultrashort pulse driving. The results show that the I–V curve presents an exponential growth trend, and the F–N curve presents two slopes because of the loss of voltage and weakening of electric field strength. The characteristics of X-ray waveform are affected by grid voltage amplitude and pulse width. The X-ray waveform amplitude and shape are gradually saturated when the pulse width of the power supply increases to 1000 V. With the increase of grid voltage, the amplitude increases gradually and emission delay time decreases sharply. The emission delay time decreases from 102 to 75 ns when the grid voltage increases from 600 to 650 V. The emission delay time is mainly affected by grid voltage amplitude according to the experimental results. The relative pulse spread increases with the increase of grid voltage and tends to be saturated with approximately 350 ns (±20 ns) when the grid voltage increases from 600 to 650 V. The theoretical limit frequency of this X-ray pulse emission system is approximately 2.86 MHz (1/350 ns). In conclusion, through analyzing deeply, the characteristic of the CNT cold cathode X-ray source is mainly affected by the grid voltage and pulse width of pulse power supply, and the X-ray detector is also a factor of X-ray waveform shape.

CRediT authorship contribution statement

Sheng Lai: Writing – review & editing, Writing – original draft, Investigation, Formal analysis, Data curation. **Yunpeng Liu:** Writing – review & editing, Supervision, Resources. **Junxu Mu:** Writing – review & editing. **Zhaopeng Feng:** Data curation. **Kai Miao:** Writing – review & editing. **Xiaobin Tang:** Writing – review & editing, Supervision, Resources, Funding acquisition.

Declaration of competing interest

The authors declare that they have no known competing financial interests or personal relationships that could have appeared to influence the work reported in this paper.

Data availability

Data will be made available on request.

References

[1] H. Li, X.B. Tang, S. Hang, Potential application of X-ray communication through a plasma sheath encountered during spacecraft reentry into earth's atmosphere, J. Appl. Phys. 121 (2017), 123101, https://doi.org/10.1063/1.4978758.

[2] J.X. Mu, X.B. Tang, Y.P. Liu, High penetration X-ray communication under physical shielding, J. X Ray Sci. Technol. 28 (2019) 187–196, https://doi.org/10.3233/XST-190587.

[3] S. Park, J.T. Kang, J.W. Jeong, A fully closed NanoFocus X-ray source with carbon nanotube field emitters, IEEE Electron. Device Lett. 39 (2018) 1936–1939, https://doi.org/10.1109/LED.2018.2873727.

[4] H.H. Huang, T. Nagashima, W.H. Hsu, Dual THz wave and X-ray generation from a water film under femtosecond laser excitation, Nanomaterials 8 (2018) 523, https://doi.org/10.3390/nano8070523.

[5] J.W. Jeong, J.W. Kim, J.T. Kang, A vacuum-sealed compact xray tube based on focused carbon nanotube field-emission electrons, Nanotechnology 24 (2016), 085201, https://doi.org/10.1088/09574484/24/8/085201.

[6] Z.P. Feng, Y.P. Liu, J.X. Mu, Optimization and testing of groove-shaped grid-controlled modulated X-ray tube for X-ray communication, Nucl. Instrum. Methods A. 1026 (2022), 166218, https://doi.org/10.1016/j.nima.2021.166218.

[7] G.A. Timofeev, N.N. Potrakhov, A.I. Nechaev, Experimental research of the x-ray communication system, in: 5th International Conference on X-Ray, Electrovacuum and Biomedical Technique, 2019, 020020, https://doi.org/10.1063/1.5095749.

[8] H. Kato, B.E. O'Rourke, R. Suzuki, Development of an Xray tube for irradiation experiments using a field emission electron gun, Nucl. Instrum. Methods A. 807 (2016) 41–46, https://doi.org/10.1016/j.nima.2015.10.080.

[9] Y. Zhang, Y.M. Tan, L.Z. Wang, Electron emission and structure stability of carbon nanotube cold cathode driven by millisecond pulsed voltage, Vacuum 172 (2020), 109071, https://doi.org/10.1016/j.vacuum.2019.109071.

[10] J.T. Kang, H.R. Lee, J.W. Jeong, Fast and stable operation of carbon nanotube field-emission X-ray tubes achieved using an advanced active-current control, IEEE Electron. Device Lett. 36 (2015) 1209–1211, https://doi.org/10.1109/LED.2015.2478157.

[11] G.Z. Yue, Q. Qiu, B. Gao, Generation of continuous and pulsed diagnostic imaging x-ray radiation using a carbon-nanotube-based fieldemission cathode, Appl. Phys. Lett. 81 (2002) 355, https://doi.org/10.1063/1.1492305.

[12] W. Lei, Z.Y. Zhu, C.Y. Liu, High-current field-emission of carbon nanotubes and its application as a fast-imaging X-ray source, Carbon 94 (2015) 687–693, https://doi.org/10.1016/j.carbon.2015.07.044.

[13] J.S. Han, S.H. Lee, H. Go, High-performance cold cathode X-ray tubes using a carbon nanotube field electron emitter, ACS Nano 16 (2022) 10231–10241, https://doi.org/10.1021/acsnano.2c02233.

[14] Golden engineering, Inc. https://www.goldenengineering.com/wp-content/uploads/2017/02/XRS4_20V_SPECSHEET_FB_JUNE2018.pdf.

[15] S. Lai, X.B. Tang, Y.P. Liu, X-ray high frequency pulse emission characteristic and application of CNT cold cathode x-ray source, Nanotechnology 33 (2021), 075201, https://doi.org/10.1088/13616528/ac378b.

[16] R. Cunningham, C. Zhao, N. Parab, Keyhole threshold and morphology in laser melting revealed by ultrahigh-speed x-ray imaging, Science 363 (2019) 849–852, https://doi.org/10.1126/science.aav4687.

[17] R. Thomson, C. Leburn D. Reid, Ultrafast Material Science Probed Using Coherent X-Ray Pulses from High-Harmonic Generation, Springer International Publishing, Berlin, 2013.

[18] Y.P. Liu, P. Dang, X.B. Tang, Performance analysis of LYSO–SiPM detection module for X-ray communication during spacecraft reentry blackout, Nucl. Instrum. Methods A. 1013 (2021), 165673, https://doi.org/10.1016/j.nima.2021.165673.

[19] P.G. Collins, A. Zettl, Unique characteristics of cold cathode carbon-nanotube-matrix field emitters, Phys. Rev. B 55 (1997) 9391–9399, https://doi.org/10.1103/PhysRevB.55.9391.

[20] S.D. Liang, Quantum Tunneling and Field Electron Emission Theories, World Scientific Publishing Co. Pte. Ltd., Singapore, 2014.

[21] The editors of encyclopaedia britannica. https://www.britannica.com/science/gamma-decay.

[22] M.J. Weber, Scintillation: mechanisms and new crystals, Nucl. Instrum. Methods A. 527 (2004) 9–14, https://doi.org/10.1016/j.nima.2004.03.009.

[23] G. Cho, H. Kim, W.S. Sul, Optimum design of quenching capacitor integrated silicon photomultipliers for TOF-PET application, in: 2nd International Conference on Technology and Instrumentation in Particle Physics, TIPP), 2012, pp. 1511–1517, https://doi.org/10.1016/j.phpro.2012.05.327.